

**Figure 2** The orientations of the unit vectors  $\hat{k}_j = k_j/k_j$  and  $\hat{P}_j = P_j/P_j (j \in [1,4])$  in the  $xz$  plane for  $\kappa = 4k_0, \epsilon = 3, \epsilon_g = 1, \epsilon_z = 2.5, \xi = 10, \xi_g = 6, \xi_z = 7, \mu = 2, \mu_g = 0.5$  and  $\mu_z = 1.5$ . [Color figure can be viewed in the online issue, which is available at [www.interscience.wiley.com](http://www.interscience.wiley.com)]

## ACKNOWLEDGMENTS

During part of this study TGM was supported by the Royal Society of Edinburgh/Scottish Executive Support Research Fellowship. AL thanks the Charles Grover Binder Endowment at Penn State for partial support.

## REFERENCES

1. T.G. Mackay, Linear and nonlinear homogenized composite mediums as metamaterials, *Electromagnetics* 25 (2005), 461–481.
2. T.G. Mackay and A. Lakhtakia, Electromagnetic fields in linear bi-anisotropic mediums, *Prog Optics*, in press.
3. A. Lakhtakia, *Beltrami fields in chiral media*, World Scientific, Singapore, 1994.
4. B. Lax and K.J. Button, *Microwave ferrites and ferrimagnetics*, McGraw-Hill, New York, 1962.
5. R.E. Collin, *Foundations for microwave engineering*, McGraw-Hill, New York, 1966.
6. W.S. Weiglhofer, A. Lakhtakia, and B. Michel, On the constitutive parameters of a chiro-ferrite composite medium, *Microwave Opt Technol Lett* 18 (1998), 342–345.
7. W.S. Weiglhofer and T.G. Mackay, Numerical studies of the constitutive parameters of a chiroplasma composite medium, *Arch Elektron Übertrag* 54 (2000), 259–265.
8. T.G. Mackay and A. Lakhtakia, Planewaves with negative phase velocity, *Phys Rev E* 69 (2004), 026602.
9. A. Lakhtakia, V.V. Varadan, and V.K. Varadan, A parametric study of microwave reflection characteristics of a planar achiral-chiral interface, *IEEE Trans Electromagn Compat* 28 (1986), 90–95.
10. T.G. Mackay, Planewaves with negative phase velocity in isotropic chiral mediums, *Microwave Opt Technol Lett* 45 (2005), 120–121; erratum 47 (2005), 406.
11. A. Baev, M. Samoc, P.N. Prasad, M. Krykunov, and J. Autschbach, A quantum chemical approach to the design of chiral negative index materials, *Opt Exp* 15 (2007), 5730–5741.
12. S.A. Ramakrishna, Physics of negative refractive index materials, *Rep Prog Phys* 68 (2005), 449–521.
13. C. Zhang and T.J. Cui, Negative reflections of electromagnetic waves in chiral media, *arXiv:physics/0610172*.
14. M. Faryad and Q.A. Naqvi, Cylindrical reflector in chiral medium supporting simultaneously positive phase velocity and negative phase velocity, *J Electromagn Waves Appl* 22 (2008), 563–572.
15. Y. Wang, X. Zha, and J. Yan, Reflection and refraction of light at the interface of a uniaxial bicrystal, *Europhys Lett* 72 (2005), 830–836.
16. N. Engheta, D.L. Jaggard, and M.W. Kowarz, Electromagnetic waves in Faraday chiral media, *IEEE Trans Antennas Propagat* 40 (1992), 367–374.
17. W.S. Weiglhofer and A. Lakhtakia, The correct constitutive relations of chiroplasmas and chiroferrites, *Microwave Opt Technol Lett* 17 (1998), 405–408.
18. J. Gerardin and A. Lakhtakia, Conditions for Voigt wave propagation in linear, homogeneous, dielectric mediums, *Optik* 112 (2001), 493–495.

© 2008 Wiley Periodicals, Inc.

## A 60 GHz MULTIPOINT FRONT-END ARCHITECTURE WITH INTEGRATED PHASED ANTENNA ARRAY

E. Moldovan, S. O. Tatu, and S. Affes

Institut National de Recherche Scientifique, Énergie Matériaux et Télécommunications, laboratoire RF, 800 de la Gauchetière Ouest, Montréal, Québec, H5A 1K6, Canada; Corresponding author: moldovan@emt.inrs.ca

Received 27 September 2007

**ABSTRACT:** A new front-end architecture dedicated to 60 GHz high-speed short-range communications is proposed. Multipoint circuits based on hybrid couplers are intensively used for both phased antenna array and down-conversion. The front-end, integrated in planar technology on ceramic substrate, use several IF quadrature conversion circuits, corresponding to multiple directions of arrival. © 2008 Wiley Periodicals, Inc. *Microwave Opt Technol Lett* 50: 1371–1376, 2008; Published online in Wiley InterScience ([www.interscience.wiley.com](http://www.interscience.wiley.com)). DOI 10.1002/mop.23367

**Key words:** millimeter-wave receivers; front-end; phased antenna array; multipoint; heterodyne

## 1. INTRODUCTION

The 7 GHz unlicensed band around 60 GHz offers the opportunity for many communication services requiring high data-rate to move toward millimeter-wave frequencies [1]. Millimeter-wave wireless personal networks (WPAN) will be designed to provide short-range, high-speed multimedia data services to terminals in rooms or office space [2]. As known, compared to the circuits at the lower-end of the microwave spectrum, millimeter-wave circuits have the advantage of miniaturization due to the increased operating frequency. Moving to higher frequencies also reduces the antenna dimensions, which are inversely proportional to carrier frequency. Therefore, an antenna array can be used in order to increase the overall gain with respect of compact size.

There are many challenges for the millimeter-wave circuits such as the necessity of low-cost and high power-efficiency, and of accurate models using computer aided design. Because of the shorter wavelength, a good circuit design must be less influenced by the inherent fabrication errors. Various millimeter-wave front-end architectures, fabrication technologies, and modulation schemes were proposed in recent years.

Monolithic microwave integrated circuit (MMIC) technology becomes a viable option for 60 GHz wireless systems. Millimeter-wave circuits for a 60 GHz front-end have been initially designed in commercial  $0.14 \mu\text{m}$  GaAs pHEMT [3] and  $0.25 \mu\text{m}$  SiGe HBT technologies [4]. The CMOS technology is the MMIC lowest cost option, and, with its rapid improvement due to continual scaling, it becomes viable to address millimeter-wave market. A fully integrated CMOS solution has the potential to drastically reduce costs enough to hit consumer price points. Various design for future 60 GHz CMOS radios are presented in [5]. A 60 GHz direct conversion receiver using conventional circuits and architectures has been recently designed in  $0.13\text{-}\mu\text{m}$  CMOS technology [6]. With a  $f_T$  of 75 GHz, the receiver would suffer from poor performance unless passive resonant devices are exploited in the design. This front-end has a noise figure of 12.5 dB and an overall gain of 28 dB. The author suggests the use of two antennas and receivers operating in parallel in order to achieve the required signal to noise ratio.

Monolithic hybrid microwave integrated circuit (MHMIC) technology remains the lowest cost option for prototype or small-scale millimeter-wave circuit fabrication. A compact integrated antenna with direct quadrature conversion using a sub-harmonic mixer operating at 40 GHz is proposed in [7]. The use of anti-parallel diode conventional mixer determinates a relatively poor overall conversion gain (RF to baseband) of  $-14.6$  dB using a high 20 GHz LO power of 11.8 dBm. However, this type of front-end containing microstrip patch antenna and related down-converter on the same ceramic substrate enables a simple, compact, lightweight, and low-cost design of millimeter-wave transceivers. A subharmonic self-oscillating mixer with integrated quasi-Yagi antenna for 60 GHz wireless applications is proposed in [8]. This is a compact planar microstrip design on 5 mil alumina substrate, having an overall conversion gain of  $-15$  dB. The 30 GHz LO dielectric resonator uses two HEMT transistors wire-bonded to the substrate.

On the basis of the previous remarks, we can conclude that a low-cost millimeter-wave front-end prototype employing antenna array is suitable to be designed on planar substrate in MHMIC technology. The antenna array with adaptive electronically steerable beams will allow mobility, and easy setup compared to directional one using fixed high gain. On the basis of our previous expertise [9–11], we propose the use of multiport circuits for both antenna array and down-converters. The multiport down-convert-

ers will reduce the required LO power comparing to conventional millimeter-wave ones. The phased antenna array will provide high directivity and an increased overall gain of the front-end compared to previous low-cost microstrip implementations. In addition, the new front-end architecture using antenna array and multiple down-converters, as presented in this article, will achieve better signal to noise performances.

## 2. PROPOSED FRONT-END ARCHITECTURE

The proposed 60 GHz receiver is designed to achieve an output signal to noise ratio  $(C/N)_{\text{out}}$  of at least 10 dB, for up to 1 Gb/s data-rate at 10 m maximum range, according to the IEEE 802.15.3c standard [1].

As known, the minimum required input signal power to obtain a specified signal to noise ratio is expressed by:

$$P_r = K[T_A + (F - 1)T_0]B\left(\frac{C}{N}\right)_{\text{out}} \quad (1)$$

In the previous equation,  $K$  is the Boltzmann constant and  $T_0$  is the room temperature. Assuming a receiver overall noise figure  $F = 12$  dB, a bandwidth  $B = 1$  GHz and an antenna temperature  $T_A = 300$  K, a minimum input signal power of  $-62$  dBm is necessary to obtain the required signal to noise ratio.

In addition, millimeter-wave communications have additional propagation losses compared to microwave communications for fixed antenna gains. Assuming simple line-of-sight free-space communication and using Friis equation, the received signal power is:

$$P_r = \left(\frac{\lambda_0}{4\pi R}\right)^2 G_t G_r P_t = A_{fs} G_t G_r P_t \quad (2)$$

In this equation,  $P_r$  depends on the transmitter power  $P_t$ , the transmitter and receiver antenna gains,  $G_t$  and  $G_r$ , and the free-space loss factor  $(\lambda_0/4\pi R)^2$  which takes into account the losses due to the spherical spreading of the energy by the antenna;  $R$  and  $\lambda_0$  represent the distance between the transmitter and receiver, and the free-space wavelength, respectively. Therefore, an additional 20-dB loss is expected for a system operating at 60 GHz compared to 6 GHz. At 60 GHz the free-space attenuation  $A_{fs}$  is as high as 68 dB for 1 m and 88 dB for 10-m range.

Using the previous results, we can conclude that, with a maximum transmitter power  $P_t$  of  $+10$  dBm [1], the minimum required input signal can be obtained at 10-m range if the gain of antennas is at least 8 dB. Fortunately, the antenna gain can be improved using antenna array. Because of the reduced wavelength of millimeter-wave signals, these arrays are small enough to be directly integrated into a planar substrate. The main benefits of the antenna array architecture are the increased gain and high directivity (essential to support very high data-rates at typical indoor distances), and the spatial diversity that it provides.

Figure 1 shows the schematic view of the geometrical model of the four-element planar antenna array. The patch antennas are spaced by  $\lambda_0/2$ , where  $\lambda_0$  is the free-space wavelength. Because of the angle of arrival  $\theta$ , a difference between two propagation paths,  $\Delta x$ , will appear. Consequently, the RF input signals will be phase shifted one versus the other by an angle  $\Delta\phi$ . As known, this phase shift is directly related to the path difference which is expressed as:

$$\Delta x_i = \lambda_0 \cdot \frac{\Delta\phi_i}{2\pi}, i = 2 \text{ to } 4 \quad (3)$$

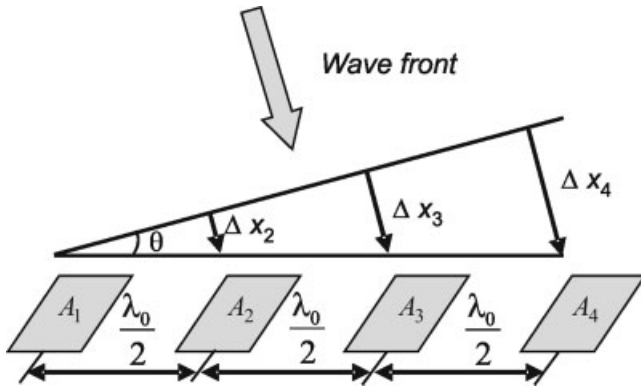


**Figure 1** The schematic view of the geometrical model of four element antenna array

Using the previous equation and the geometrical model of Figure 1, the angle of arrival can be obtained as:

$$\sin \theta = \frac{\Delta x_i}{(i-1) \frac{\lambda_0}{2}} = \frac{\Delta \phi_i}{(i-1) \pi}, i = 2 \text{ to } 4 \quad (4)$$

Figure 2 shows the block diagram of a four element antenna array. Its architecture is based on a  $4 \times 4$  Butler matrix having an original topology adapted to millimeter-wave frequencies, which avoids any cross line [12]. The four patch antennas are connected to a multiport circuit having four inputs and four outputs. This circuit is composed of four  $90^\circ$  hybrid couplers and two  $45^\circ$  phase shifters, realized using  $\lambda_g/8$  transmission lines. Because of their small dimensions, the patch antennas are integrated on the same substrate.

To calculate the multiport output signals,  $b_5$  to  $b_8$ , the pattern factor of a patch antenna in the  $H$ -plane is considered [13]:

$$F_H(\theta) = \cos \theta \cdot \frac{\sin \left[ \frac{\beta \cdot W}{2} \cdot \sin \theta \right]}{\frac{\beta \cdot W}{2} \cdot \sin \theta} \quad (5)$$

In this equation,  $\beta$  is the free-space propagation constant and  $W$  is the patch width, selected to obtain a proper radiation resistance  $R$  to the input ( $W = \lambda_g/2 = \lambda_0/(2\sqrt{\epsilon_{\text{eff}}})$ ;  $R = 50 \Omega$ ). Hence, the previous equation becomes:

$$F_H(\theta) = \cos \theta \cdot \frac{\sin \left[ \frac{\pi}{2\sqrt{\epsilon_{\text{eff}}}} \cdot \sin \theta \right]}{\frac{\pi}{2\sqrt{\epsilon_{\text{eff}}}} \cdot \sin \theta} \quad (6)$$

According to Eqs. (3) and (4), and the geometrical model of Figure 1, the four input signals of the multiport antenna array,  $a_1$  to  $a_4$ , are:

$$a_i = a \exp(-j\Delta \phi_i) \cdot F_H(\theta) = a \exp[-j(i-1)\pi \cdot \sin \theta] \cdot F_H(\theta), \quad i = 1 \text{ to } 4 \quad (7)$$

The  $S$  matrix of the  $90^\circ$  hybrid coupler is given by the following equation:

$$[S] = \frac{1}{\sqrt{2}} \begin{bmatrix} 0 & j & 1 & 0 \\ j & 0 & 0 & 1 \\ 1 & 0 & 0 & j \\ 0 & 1 & j & 0 \end{bmatrix} \quad (8)$$

Based on the block diagram of Figure 2, the four multiport output signals are:

$$b_5 = \frac{1}{2} (-a_1 \cdot e^{-j\frac{\pi}{4}} + ja_2 + ja_3 \cdot e^{-j\frac{\pi}{4}} + a_4) \cdot F_H(\theta) \quad (9)$$

$$b_6 = \frac{1}{2} (ja_1 + ja_2 \cdot e^{-j\frac{\pi}{4}} - a_3 + ja_4 \cdot e^{-j\frac{\pi}{4}}) \cdot F_H(\theta) \quad (10)$$

$$b_7 = \frac{1}{2} (ja_1 \cdot e^{-j\frac{\pi}{4}} - a_2 + a_3 \cdot e^{-j\frac{\pi}{4}} + ja_4) \cdot F_H(\theta) \quad (11)$$

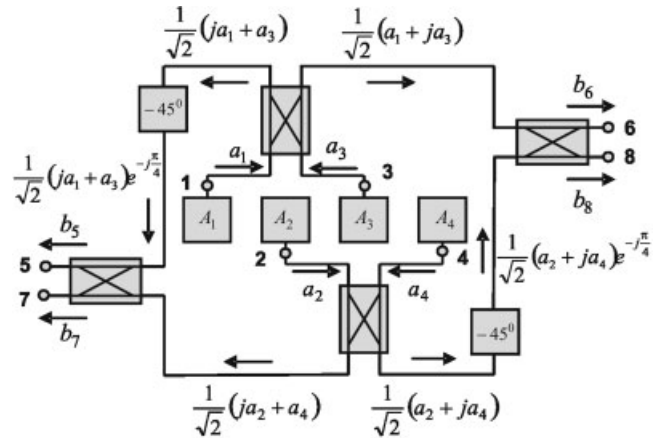
$$b_8 = \frac{1}{2} (a_1 + ja_2 \cdot e^{-j\frac{\pi}{4}} + ja_3 - a_4 \cdot e^{-j\frac{\pi}{4}}) \cdot F_H(\theta) \quad (12)$$

Figure 3 shows the computed normalized output signals versus the angle of arrival using the previous equations. For each output signal, an individual maximum is obtained by shifting  $\theta$  in  $180^\circ$  range. The side-lobes are at least 8 dB below the main lobe and the angles of arrival corresponding to maximum signals are around:  $-45^\circ$ ,  $-15^\circ$ ,  $15^\circ$ , and  $45^\circ$ . Therefore, the main lobe of the antenna array can be shifted by  $30^\circ$  multiples. The phased array outputs can be used as inputs into a multiple-input multiple-output (MIMO) millimeter-wave front-end.

The second multiport is the key component of the millimeter-wave down-converter. The block diagram of this circuit with corresponding signals is presented in Figure 4. This circuit uses the same hybrid coupler as the multiport antenna array. We note that the LO millimeter-wave is connected at Port 5 and the RF input is injected to Port 6. As previously demonstrated in [10, 11],  $I/Q$  down-conversion is performed using power detectors and differential amplifiers:

$$i(t) = K_1 \cdot (|b_3|^2 - |b_1|^2) = K_2 \cdot \alpha(t) \cdot |a|^2 \cdot \cos[\Delta \varphi(t)] \quad (13)$$

$$q(t) = K_1 \cdot (|b_4|^2 - |b_2|^2) = K_2 \cdot \alpha(t) \cdot |a|^2 \cdot \sin[\Delta \varphi(t)] \quad (14)$$



**Figure 2** The block diagram of the antenna array based on multiport circuits

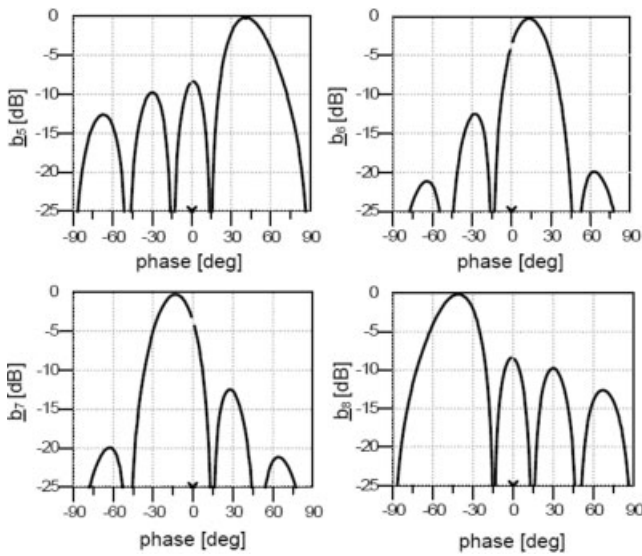


**Figure 3** Computed normalized multiport antenna array output signals versus the angle of arrival

The quadrature signals are function of the instantaneous amplitude ratio  $\alpha(t)$  and the phase shift  $\Delta\varphi(t)$  between the RF input signals. Their amplitudes depend on the millimeter-wave LO amplitude,  $a$ , and of some constants,  $K_1$  and  $K_2$ . Therefore, the demodulation of MPSK or QAM signals is directly performed.

A typical block diagram of a millimeter-wave heterodyne receiver which uses the second multiport, MP 2, is illustrated in Figure 5. Because of its performance, the use of this architecture is suitable for a low-cost millimeter-wave receiver. First, millimeter-wave multiport down-converter, MP DC, requires a reduced LO power by at least 10–15 dB compared with conventional architectures [14]. A maximum millimeter-wave LO power of  $-10$  dBm is enough to achieve excellent down-conversion results. Second, using a heterodyne architecture, the millimeter-wave LO drift can be easily compensated using a loop signal (generated by the signal processing SP block of the IF demodulator, IF D) connected to the second LO. Therefore, a costly millimeter-wave LO can be avoided without reducing the system performance. Finally, this

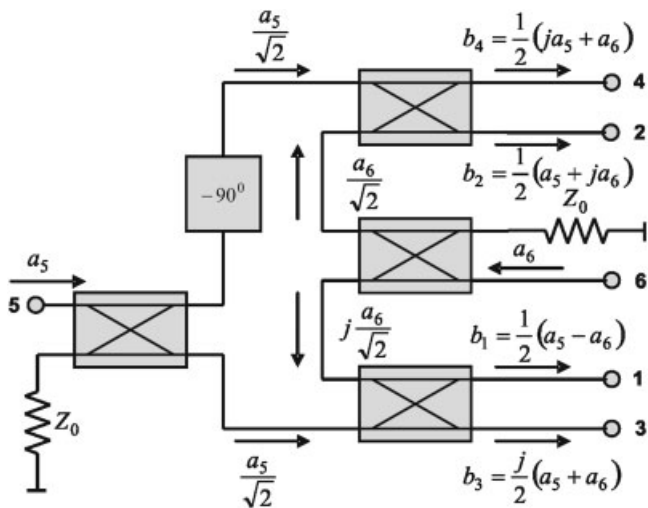


**Figure 4** The block diagram of the multiport circuit used for millimeter-wave down-converter

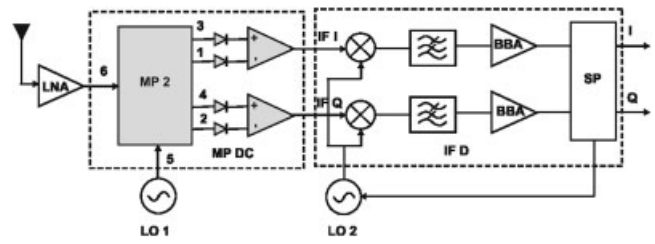


**Figure 5** The simplified block diagram of the millimeter-wave heterodyne receiver

heterodyne architecture can provide the receiver required overall gain of around 70 dB.

The block diagram of a 60 GHz MIMO receiver using the proposed multiport front-end is presented in Figure 6. The multiport antenna array, MP 1, is connected directly to four identical multiport down-converters. This low-cost implementation of the millimeter-wave front-end contains only passive circuits and the related power detectors, excepting the millimeter-wave local oscillator. Therefore, the overall noise figure will increase because no LNA is used. The expected value of the noise figure  $F$  is around 19 dB. According to Eqs. (1) and (2), and considering the same antenna gains, the bandwidth must be reduced to 200 MHz to obtain the same  $C/N$  ratio of 10 dB for a WPAN maximum range of 10 m. However, the bandwidth (and related data-rate) can increase at 500 MHz or 1 GHz for 7- or 4-m range, respectively, by keeping the same  $C/N$  ratio. Hardware improvements such as an increased antenna gain, reduced insertion and down-conversion losses (signifying a reduced  $F$ ), and advanced modulation schemes

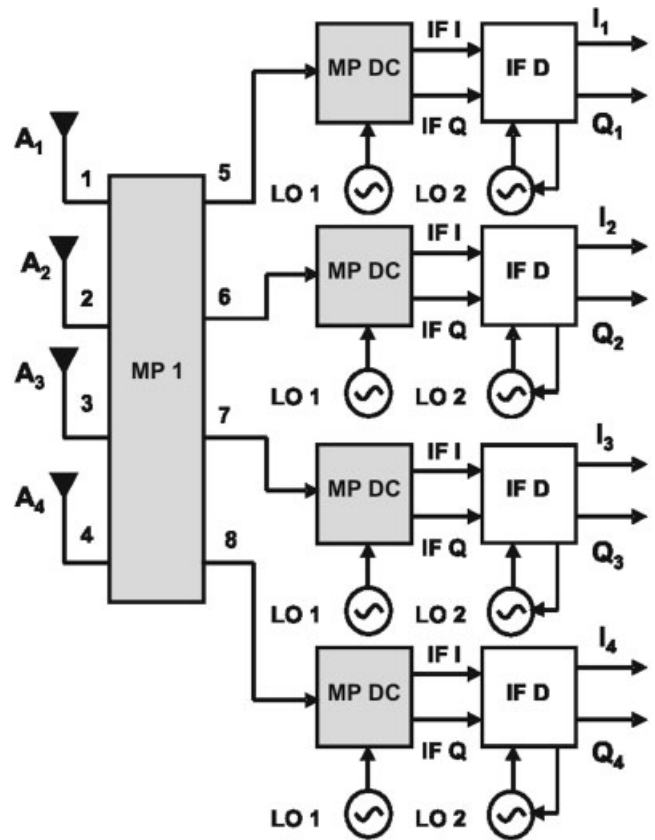


**Figure 6** The simplified block diagram of the proposed antenna array millimeter-wave receiver

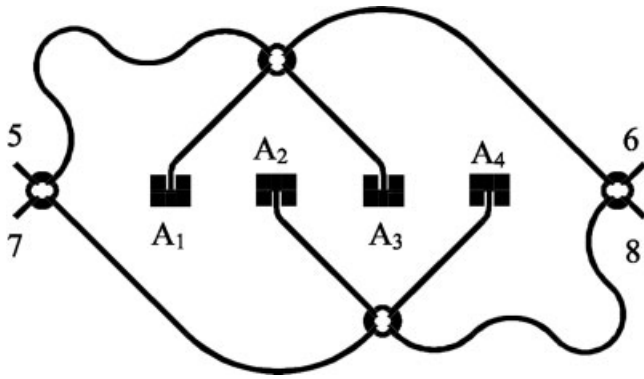


**Figure 7** The lay-out of the proposed antenna array based on multiport circuit

will allow higher data-rates using this proposed low-cost architecture. In addition, the BER can be also reduced by appropriate signal processing techniques, even if the  $C/N$  ratio decreases due to an increasing data-rate.

### 3. MILLIMETER-WAVE MULTIPORTS

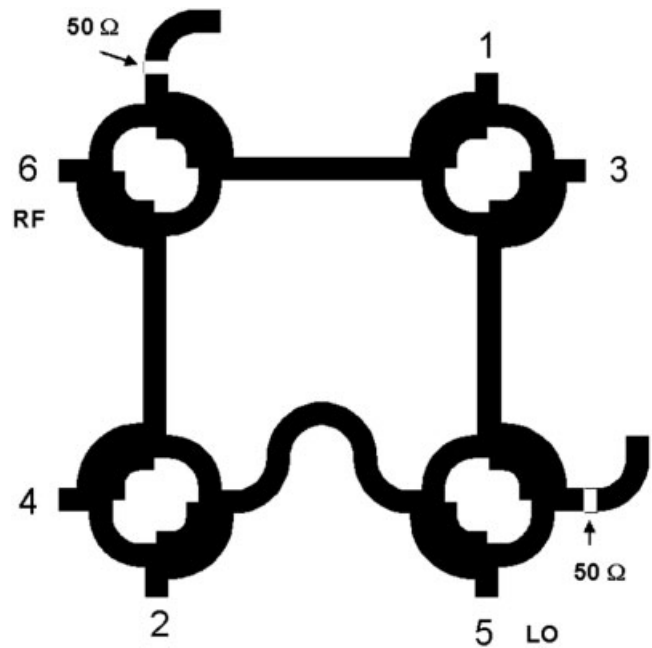
Multiport circuits are designed on MHMIC technology using a ceramic substrate of 9.9 relative permittivity and  $125 \mu\text{m}$  thickness. As shown in Figures 2 and 4, the multiports are composed of hybrid couplers and transmission lines. The required phase shifts are obtained using appropriate length of the transmission lines which interconnect these couplers. The central frequency was chosen at 61 GHz.

Figure 7 shows the lay-out of the proposed multiport antenna array based on the block diagram of Figure 2. Antenna patches are spaced by  $\lambda_0/2 = 2.45 \text{ mm}$  and connected to hybrid couplers. The antennas are placed in opposite position, alternatively, in order to decrease losses by avoiding cross lines. The lengths of transmission lines are critical and are optimized by successive advanced design system (ADS) Momentum simulations, in order to obtain required transmission  $S$  parameter phases. A rounded geometry of the  $90^\circ$  hybrid coupler, instead of the conventional squared one, is used to improve  $S$  parameter performances over the frequency band. Its return losses and isolations are less than  $-30 \text{ dB}$  in a 1 GHz band, and an equal power split having a supplementary insertion loss of  $0.25 \text{ dB}$  is obtained exactly at the central frequency. The phase difference between the two output ports is exactly  $90^\circ$  over more than 2 GHz band. Furthermore, all the connection lines are also rounded to avoid corner reflections. Therefore, the overall multiport  $S$  parameters are excellent in a 1 GHz frequency band. The size of whole multiport is 9 mm by 14 mm.

Each output of the multiport antenna array is directly connected to a multiport down-converter, which uses the same  $90^\circ$  hybrid coupler. The lay-out of the MP 2 is presented in Figure 8. The size of this multiport is 3 mm by 3 mm. The IF signals are generated using power detectors (Schottky diodes) connected at multiport outputs, as seen in Figure 5.

We note that it is possible to integrate all components of the millimeter-wave front-end on the same ceramic substrate. The LO signal can be injected at corresponding MP 2 inputs and split using Wilkinson power dividers or hybrid couplers. The estimated size of millimeter-wave front-end, excepting the LO, is around 10 mm by 20 mm.

Multiport antenna array ADS Momentum post-processing 2D visualizations show four distinct beams located at  $-45^\circ$ ,  $-15^\circ$ ,



**Figure 8** The lay-out of the second multiport circuit

$15^\circ$ , and  $45^\circ$ , as previously computed using Eqs. (9) to (12). The 2D normalized radiation patterns are illustrated in Figure 9 for the corresponding input signals  $a_5$  to  $a_8$ . Each radiation pattern is obtained considering a single port excitation, indicated on the corresponding pattern. The other ports are connected to  $50\text{-}\Omega$  loads. As seen, the side-lobes are at least 10 dB below the main lobe. Momentum post-processing analysis shows corresponding antenna array gains of 8.3, 7.4, 7.4, and 8.3 dB, respectively. Considering that the antenna array is used in a front-end receiver, if the direction of arrival is  $+45^\circ$ , the corresponding gain is 8.3 dB and the optimum antenna array output is Port 5. If the angle of arrival increases by  $30^\circ$  multiples, the optimum outputs are to Ports 6–8, respectively. Compared to the antenna proposed in [12], even if the operation frequency is increased by 50%, the antenna array  $S$  parameter performances are improved by adopting an appropriate design of components at millimeter-wave frequen-

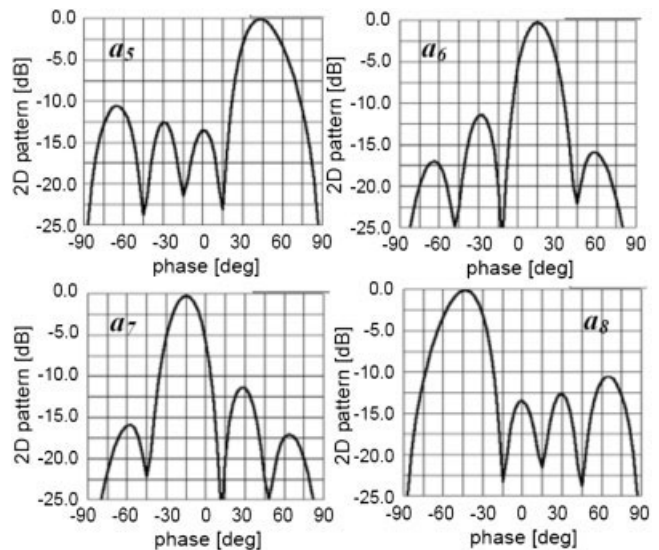


**Figure 9** Simulated 2D normalized radiation patterns of antenna array

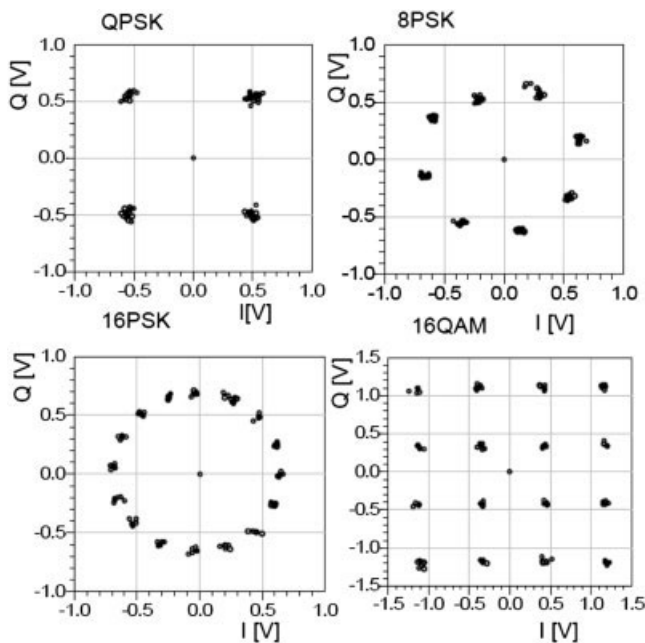


**Figure 10** Demodulation results of high-speed MPSK/QAM signals using proposed multiport heterodyne architecture

cies. Improved performances are also obtained in terms of side-lobe levels (less than  $-10$  dB versus  $-7$  dB in [12]) and the scan sector of the array ( $90^\circ$  versus  $62^\circ$  in [12]). Simulation results show a very good match with the theoretical ones in terms of the number, the level, and the direction of the side-lobes.

Supposing a perfect synchronism and no additional noise, Figure 10 shows various simulation results of the demodulated constellations using the proposed multiport heterodyne architecture for various high-speed MPSK/QAM signals: 100 Mb/s for QPSK, 200 Mb/s for 8PSK and 16 QAM, and 400 Mb/s for 16PSK. As seen, all clusters of the demodulated constellations are very well positioned and individualized. Because of the differential approach and the multiport design, the DC offset represented by the distance between the central point and the origin is almost zero. To cope with data-rates between 100 and 400 Mb/s, the IF of the heterodyne receiver was chosen at 900 MHz. If the data-rate is increased to 1 Gb/s, the IF can be chosen at 2.45 or 5.8 GHz.

The second frequency conversion uses conventional mixers according to the block diagram of Figure 5. Simulated BER results are also excellent, even if an important millimeter-wave LO frequency error from synchronism (up to 25 MHz, dynamically compensated using the second LO) is considered. The BER values are less than  $10^{-5}$  for energy per bit to noise power spectral density ( $E_b/N_0$ ) ratio of 10 dB. Compared with the direct conversion, due to the heterodyne architecture, an improved overall gain was obtained, essential to compensate the high value of free space attenuation loss at 60 GHz frequency band. These results prove that this simple multiport architecture can be suitable for low-cost millimeter-wave receivers of future 60 GHz WPAN applications.

#### 4. CONCLUSION

A new V-band millimeter-wave multiport heterodyne receiver architecture has been presented in this article. An antenna array based on a multiport circuit provides four output signals corresponding to four optimal directions of arrival. The millimeter-wave frequency conversion is obtained using the proposed I/Q multiport down-converter, avoiding the use of a costly active

mixer or a high-power millimeter-wave LO (in the case of the conventional diode mixers). Simulations show excellent demodulation results using high-speed V-band MPSK/QAM modulated signals.

The proposed multiport heterodyne architecture enables the design of compact and low-cost wireless millimeter-wave communication receivers for future high-speed wireless communication systems, according to the IEEE 802.15.3c wireless standard.

#### ACKNOWLEDGMENT

This work was financially supported by the National Science Engineering Research Council (NSERC) of Canada.

#### REFERENCES

1. R. Fisher, 60 GHz WPAN standardization within IEEE 802.15.3c, 2007 international symposium on signals, systems, and electronics, IEEE catalog Number 07EX1869C, 2007, pp. 103–105.
2. P. Smulders, Exploiting the 60 GHz band for local wireless multimedia access: Prospects and future directions, *IEEE Commun Mag* 01 (2002), 140–147.
3. H. Zirath, C. Fager, M. Garcia, L.L. Sakalas, and A. Alping, Analog MMICs for millimeter-wave applications based on a commercial  $0.14\text{-}\mu\text{m}$  pHEMT technology, *IEEE Trans Microwave Theory Tech* 49 (2001), 2086–2092.
4. W. Winkler, 60 GHz transceiver circuits in SiGe HBT technology, *IEEE Compd Semicond Integr Circ Symp* (2005), 109–112.
5. C.H. Doan, S. Emami, D.A. Sobel, A.M. Niknejad, and R.W. Brodersen, Design consideration for 60 GHz CMOS radios, *IEEE Commun Mag* (2004), 132–140.
6. B. Razavi, A 60-GHz CMOS receiver front-end, *IEEE J Solid-State Circ* 41 (2006), 17–22.
7. J.Y. Park, S. Leon, Y. Wang, and T. Itoh, Integrated antenna with direct conversion circuitry for broad-band millimeter-wave communications, *IEEE Trans Microwave Theory Tech* 51 (2003), 1482–1488.
8. M. Sironen, Y. Qian, and T. Itoh, A subharmonic self-oscillating mixer with integrated antenna for 60 GHz wireless applications, *IEEE Trans Microwave Theory Tech* 49 (2001), 442–450.
9. S.O. Tatu, E. Moldovan, Ke Wu, and R.G. Bosisio, A new direct millimeter-wave six-port receiver, *IEEE Trans Microwave Theory Tech* 49 (2001), 2517–2522.
10. S.O. Tatu, E. Moldovan, Ke Wu, R.G. Bosisio, and T.A. Denidni, Ka-band analog front-end for software-defined direct conversion receiver, *IEEE Trans Microwave Theory Tech* 53 (2005), 2768–2776.
11. S.O. Tatu and E. Moldovan, V-band multiport heterodyne receiver for high-speed communication systems, *EURASIP J Wireless Commun Networking* 2007, 7, Article ID 34358.
12. C. Dall’Omo, T. Monediere, B. Jecko, F. Lamour, I. Wolf, and M. Elkael, Design and realization of a  $4 \times 4$  microstrip butler matrix without any crossing in millimeter waves, *IEEE Microwave Opt Technol Lett* 38 (2003), 462–465.
13. W.L. Stutzman and G.A. Thiele, *Antenna theory and design*, 2nd ed., Artech House, New York, 1997.
14. D. Hammou, N. Mallat, E. Moldovan, S. Affes, Ke Wu, and S.O Tatu, V-band six-port down-conversion techniques, 2007 International symposium on signals, systems, and electronics, IEEE catalog Number 07EX1869C, 2007, pp. 379–382.

© 2008 Wiley Periodicals, Inc.